Kinetic analysis of distinct product generation in oxidative pyrolysis of four octane isomers

Kun Wang[1*], C. T. Bowman[1] and H. Wang[1]

[1] *Mechanical Engineering Department, Stanford University, Stanford, California 94305-3032, USA*

Corresponding Author:

Kun Wang
Stanford University
Mechanical Engineering Department
452 Escondido Mall
Building 520, Room 215
Stanford, California 94305-3032, USA
Phone: 650-497-0433
Fax: 650-723-1748
Email: kwang5@stanford.edu

Colloquium Topic Area: REACTION KINETICS

Total length:	6102 words		
Main text =	3168 words		
References =	(20 references + 2) x (2.3 lines/reference) x (7.6 words/line) =	385	words
Table 1 =	(11 text lines + 2 lines) x (7.6 words/line) x 1 column =	99	words
Table 2 =	(11 text lines + 2 lines) x (7.6 words/line) x 2 column =	198	words
Figure 1 =	(42mm + 10 mm) x (2.2 words/mm) x 1 column =	114	words
Figure 2 =	(132mm + 10 mm) x (2.2 words/mm) x 1 column =	313	words
Figure 3 =	(61mm + 10 mm) x (2.2 words/mm) x 2 columns =	314	words
Figure 4 =	(47mm + 10 mm) x (2.2 words/mm) x 1 column =	126	words
Figure 5 =	(60mm + 10 mm) x (2.2 words/mm) x 2 columns =	309	words
Figure 6 =	(86mm + 10 mm) x (2.2 words/mm) x 2 columns =	424	words
Figure 7 =	(154mm + 10 mm) x (2.2 words/mm) x 1 column =	360	words
	Subtotal (figures)	1960	words
Fig. caption =	293 words		

Submitted for consideration at the 37th International Symposium on Combustion

and publication in the *Proceedings of the Combustion Institute*

Technical Report Documentation Page

1. Report No.	2. Government Accession No.	3. Recipient's Catalog No.
j.proci.2018.06.219		

4. Title and Subtitle	5. Report Date
Kinetic analysis of distinct product generation in oxidative pyrolysis of four octane isomers	July 2018
	6. Performing Organization Code

7. Author(s)	8. Performing Organization Report No.
Kun Wang, C. T. Bowman and H. Wang	

9. Performing Organization Name and Address	10. Work Unit No. (TRAIS)
Center of Excellence for: Alternative Jet Fuels and Environment Stanford University Mechanical Engineering Department Stanford CA 94305	11. Contract or Grant No. 13-C-AFJE-SU-006

12. Sponsoring Agency Name and Address	13. Type of Report and Period Covered
Federal Aviation Administration Office of Environment and Energy	Journal Article
	14. Sponsoring Agency Code

15. Supplementary Notes

16. Abstract

The molecular structures of hydrocarbon fuels are known to have a substantial impact on their combustion properties. However, the relationship between the fuel structure and thermal decomposition intermediate products, which determine the global combustion behaviors, is not as well known. In this study, four octane isomers, n-octane, 2,5-dimethylhexane, 2,2,4-trimethylpentane (iso-octane), and 2,2,3,3-tetramethylbutane, are selected as the model compounds to illustrate the distinct product generation in the oxidative pyrolysis of large hydrocarbons with substantially different molecular structures. Both experimental and kinetic analysis show that all the octane isomers lead to the formation of a similar group of stable products, with the major ones being ethene, methane, propene, and isobutene. The distributions of these products vary from fuel to fuel. n-Octane produces primarily ethene, while isobutene formation increases with increasing branching in the fuel molecular structure. The most branched isomer, 2,2,3,3-tetramethyl-butane, produces predominately isobutene. Lumped, two-step reaction schemes are proposed for each octane isomer. Together with a detailed foundational fuel chemistry model, it is shown that the reaction models accurately predict the formation and subsequent consumption of the intermediate products for all octane isomers studied.

17. Key Words	18. Distribution Statement
Oxidative pyrolysis; reaction kinetics; octane isomers; characteristic reaction time, ASCENT	

19. Security Classif. (of this report)	20. Security Classif. (of this page)	21. No. of Pages	22. Price
Unclassified	Unclassified		

Kinetic analysis of distinct product generation in oxidative pyrolysis of four octane isomers

Kun Wang[1*], C. T. Bowman[1] and H. Wang[1]

[1] *Mechanical Engineering Department, Stanford University, Stanford, California 94305-3032, USA*

* Corresponding author.

Abstract

The molecular structures of hydrocarbon fuels are known to have a substantial impact on their combustion properties. However, the relationship between the fuel structure and thermal decomposition intermediate products, which determine the global combustion behaviors, is not as well known. In this study, four octane isomers, *n*-octane, 2,5-dimethylhexane, 2,2,4-trimethylpentane (*iso*-octane), and 2,2,3,3-tetramethylbutane, are selected as the model compounds to illustrate the distinct product generation in the oxidative pyrolysis of large hydrocarbons with substantially different molecular structures. Both experimental and kinetic analysis show that all the octane isomers lead to the formation of a similar group of stable products, with the major ones being ethene, methane, propene, and isobutene. The distributions of these products vary from fuel to fuel. *n*-Octane produces primarily ethene, while isobutene formation increases with increasing branching in the fuel molecular structure. The most branched isomer, 2,2,3,3-tetramethyl-butane, produces predominately isobutene. Lumped, two-step reaction schemes are proposed for each octane isomer. Together with a detailed foundational fuel chemistry model, it is shown that the reaction models accurately predict the formation and subsequent consumption of the intermediate products for all octane isomers studied.

Keywords: *Oxidative pyrolysis; reaction kinetics; octane isomers; characteristic reaction time*

1. Introduction

In studies of the pyrolysis of petroleum-derived jet fuels, it has been reported that the primary decomposition product is ethene, with smaller amounts of methane and propene [1-3], while for alcohol-to-jet (ATJ) fuels the primary decomposition product is isobutene [3]. A dramatic difference between these two types of fuel is that the petroleum-derived jet fuels are a complex mixture of normal alkanes, lightly-branched *iso*-alkanes, *cyclo*-alkanes and alkylated aromatics, while the ATJ fuels comprise a small number of species that are primarily heavily-branched *iso*-alkanes. Hence, the decomposition products are highly correlated with the fuel molecular structures. Furthermore, it has been shown that during the combustion of a jet fuel, fuel pyrolysis is essentially decoupled from the oxidation of decomposed products and that the global combustion properties, such as the ignition delay and laminar flame speed, are largely determined by the distribution of the thermal decomposition products [1, 2]. A basic understanding of the influence of the molecular structures of the fuel constituents on the pyrolysis product distributions is critical to our ability to predict the combustion behaviors of jet fuels, and perhaps for that matter, all fuels of a distillate origin.

Several earlier studies revealed that for a single hydrocarbon fuel, the global, high-temperature combustion behaviors are sensitive to fuel molecular structures [4-7]. The reaction intermediates from the fuel decomposition have been observed to have an impact on the flame propagation rate [8, 9]. In this study, we explore the relationships among fuel structure, thermal decomposition product distribution, and combustion behaviors in a direct and quantitative manner, focusing on the degree of branching in *iso*-paraffins. Four octane isomers (shown in Fig. 1), with varying degrees of branching, are selected as model compounds. Four octane isomers (shown in Fig. 1), with varying degrees of branching, are selected as model compounds. They are *n*-octane (*n*-C_8H_{18}), 2,5-dimethylhexane (*d*-C_8H_{18}), 2,2,4-trimethylpentane (*i*-C_8H_{18}), and 2,2,3,3-tetramethylbutane (*t*-C_8H_{18}). To emulate fuel decomposition in combustion environments, oxidative pyrolysis experiments were performed in a flow reactor at atmospheric pressure and a temperature of 1137K. The temperature was chosen based on the results of the prior experiments [1,2].

It provides sufficient information about the product distributions to test the proposed modeling approach and to ensure the kinetic results of the four fuel reactants tested can be directly compared amongst each other. Characteristic reaction times were used to develop reaction pathways and kinetics for the distinct product generation observed for the four octane isomers.

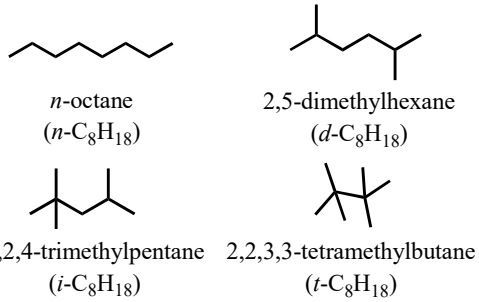

Fig. 1. Molecular structures of four octane isomers investigated in the present study.

2. Experimental method

The Stanford flow reactor facility is described in detail elsewhere [10]. The reactor is comprised of a vertical 30 cm long × 3 cm diameter quartz tube enclosed in a pressure vessel. An H_2-air premix flame is used to provide the main thermal source; electric heaters surround the reactor tube to maintain nearly isothermal conditions. Except for 2,2,3,3-tetramethylbutane, all other hydrocarbon reactants are in the liquid state at room temperature. Each of them was injected directly into a vaporizer by a syringe pump before being introduced into the reactor with a nitrogen carrier gas. 2,2,3,3-Tetramethylbutane is crystalline at room temperature. One portion of 2,2,3,3-tetramethylbutane was dissolved in two portions of toluene on a molar basis. The resulting mixture was then delivered into the reactor. A control experiment of the oxidative pyrolysis of toluene was performed, and negligible toluene conversion was observed, indicating that the solvent on its own is chemically inactive under the condition tested (see, Fig. S1 of the SPM). Table 1 summaries all the experiments and their associated conditions. The equivalence ratio of the mixture is kept at unity. The balance gas is mainly composed of nitrogen and H_2O vapor with small quantities of argon and CO_2 as the result of vitiation.

The reaction products were sampled by a cooled extraction probe that was translated along the reactor centerline using a computer controlled stepping motor. Gas samples were sent

through a heated line into a 4-column micro gas chromatograph (Inficon microGC 3000) for analysis. In addition, a non-dispersive infrared analyzer (NDIR) and a paramagnetic analyzer (PMA) were used for real-time measurements of CO, CO_2 and O_2 that could be compared with the GC data. Typical residence times in the reactor were 30 ms. The total uncertainty in species concentration is ±2 to ±5% for most species.

Table 1. Summary of oxidative pyrolysis experiments for the four octane isomers.

Compound	T (K)	P (atm)	Initial conc/ppm	ϕ	Solution
n-C_8H_{18}[a]	1137	1	501	1.0	n.a.
d-C_8H_{18}[a]	1137	1	501	1.0	n.a.
i-C_8H_{18}[a]	1137	1	501	1.0	n.a.
t-C_8H_{18}[b]	1137	1	650	1.3	toluene

The composition of the balance gas are: [a] 228ppm CO_2, 5075 Ar, 6261 O_2, 215133 H_2O, 772802 N_2; [b] 228 CO_2, 5070 Ar, 6254 O_2, 214925 H_2O, 772052 N_2, 999180 toluene.

3. Kinetic time-scale analysis and modeling

As demonstrated earlier [1, 2, 11], fuel decomposition under the conditions tested may be analyzed and treated by a lumped reaction approach. The basis of this approach is the steady-state assumption that relies on a time scale analysis of the underlying reaction processes. The characteristic reaction time for a first order reaction (e.g., the β–scission of an alkyl radical) is $\tau = 1/k$. For a bimolecular reaction A + B → products, a pseudo-first order reaction rate coefficient may be defined as $k = k'$[B], where k' is the bimolecular rate coefficient, as long as [B] is known (or assumed).

The rate parameters of the reactions relevant to octane isomers studied are obtained from literatures [12-14]. The reverse rate coefficients are obtained from equilibrium constants. The thermodynamic data are estimated using the group additivity method [15]. In constructing a lumped reaction model, USC Mech II [16] (111 species and 784 reactions) was used to account for the secondary reactions of decomposed products. Four reaction models are created for each

octane isomer studied herein. ChemKin II [17] was used for the constant-pressure, constant temperature simulations. These models would be applicable in the range of T = 700-1400 K and p = 0.1-50 atm.

4. Results

4.1. Oxidative pyrolysis experiments

Four species are found to be the major products during the oxidative pyrolysis of the four octane isomers, accounting for ~75% of total carbon mass from octane decomposition. They are methane, ethene, propene, and isobutene. Their distributions are expected to determine the global combustion properties. The time evolutions of these species are shown in Fig. 2. At least four measurements are made for each data point and the average value is reported. The one-standard deviations from all these measurements for several representative points are also shown. A more complete set of species includes hydrogen, ethane, acetylene, propyne, allene, 1-butene, carbon monoxide, and small amounts of aromatics. The fuel decay of *n*- and *i*-octane also was measured. The fuel decay for *d*- and *t*-octane are expected to be rapid (see, e.g., Fig. 7 for the simulation result for the decomposition of *t*-octane), and thus were not measured here. The mass balances of carbon and hydrogen in all experiments are >95%.

The most striking observation from Fig. 2 is that ethene and isobutene dominate the major products of *n*-C_8H_{18} and *t*-C_8H_{18}, respectively, while the differences among these products in *d*-C_8H_{18} and *i*-C_8H_{18} are smaller. With increasing branching in the molecular structure, sequentially from *n*-C_8H_{18}, to *d*-C_8H_{18}, to *i*-C_8H_{18}, and finally to *t*-C_8H_{18}, the ethene yields decreases and the isobutene yields increases. The less branched isomer *d*-C_8H_{18} produces more propene than the more branched *i*-C_8H_{18} and *t*-C_8H_{18}; the methane yields are comparable among all octane isomers. Another significant observation is that nearly no depletion of oxygen (not shown) is observed over the reaction time in all experiments, indicating that the reactions involve essentially thermal decomposition.

A closer look at Fig. 2 show that the yields for all major products increase very rapidly within the first 5 ms, with the rates of production decreasing substantially afterwards. The higher concentration of fuels during the first 5 ms is due to mixing with the balance gases at the beginning of the flow reactor. The disappearance of propene and isobutene is due to secondary reactions. The above observations are consistent with the jet fuel studies [2, 3], in that jet fuels that contain substantial *n*-alkane and lightly-branched *iso*-alkanes produces mostly ethene; while the bio-derived ATJs, which contain heavily branched hydrocarbons, produce predominantly isobutene. The somewhat different combustion properties between these two jet fuels may thus result from the different combustion behaviors of ethene and isobutene.

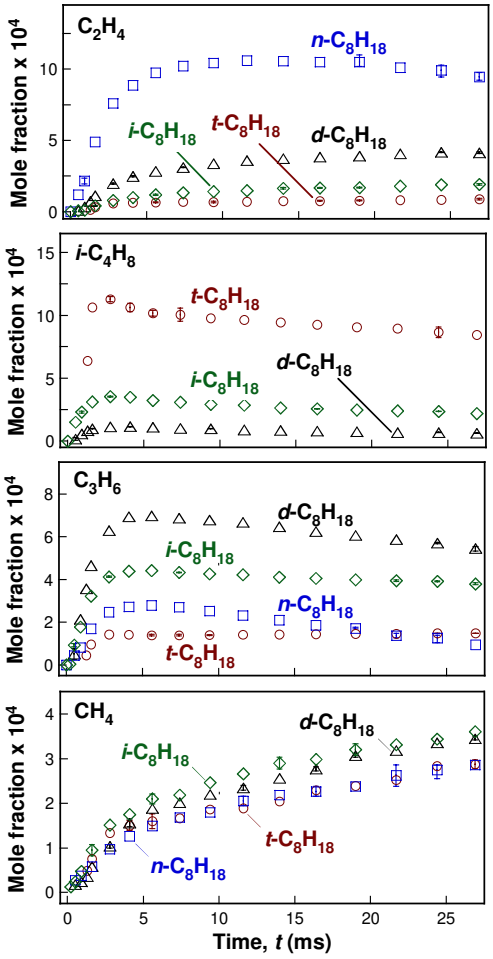

Fig. 2. Major product distributions in the oxidative pyrolysis of the four octane isomers under the conditions specified in Table 1. No isobutene was detected for *n*-C_8H_{18}.

4.2. Kinetic analysis

Normal Octane

The production of ethene from the thermal decomposition of *n*-alkane is driven by sequential *β*-scission of the alkyl radicals. For *n*-octane, the H-abstraction produces one primary and three secondary octyl radicals (Fig. 3). The energy barriers for 1,6-, 1,5- and 1,4-H-shift isomerization reactions are 15, 15 and 22 kcal/mol, respectively [13]. Along with the significant tunneling effects, the H-shift isomerization reactions are faster than the respective C–C *β*-scission of the alkyl radicals (with energy barriers slightly over 30 kcal/mol [18], while the C–H *β*-scission barrier is about 35 kcal/mol, thus being neglected in our analysis). Hence, the alkyl radicals are expected to rapidly equilibrate under the experimental condition before undergoing *β*-scission reactions. Alkyl radicals with 5 or more carbon atoms repeat the above equilibrium and *β*-scission reaction processes.

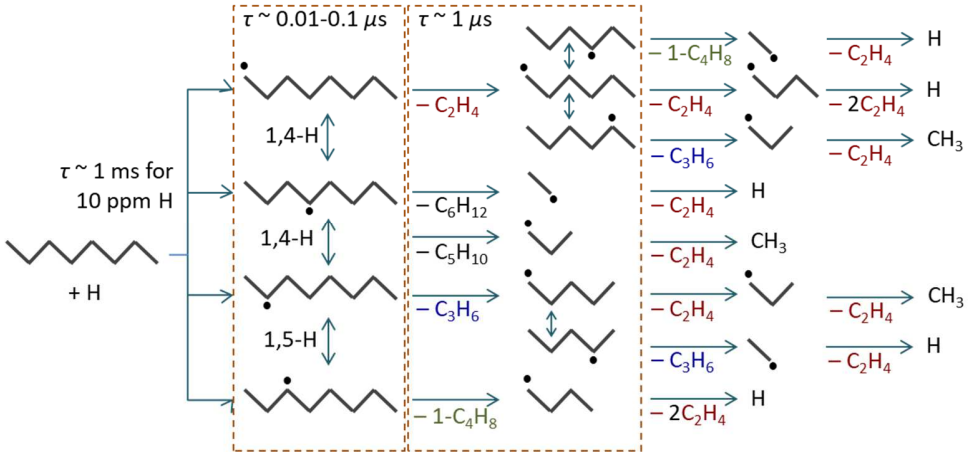

Fig. 3. Illustration of the species produced, assuming only C–C *β*-scission and neglecting C–H *β*-scission. The characteristic times are calculated for 1000 K, 1 atm with 10 ppm initial H mole fraction. The 1000 K value is chosen to simplify the analysis; analysis at other temperatures led to the same conclusion. The H atom concentration used in the calculation of the characteristic time (10 ppm) is typical for the experiment.

C–C or C–H fission reactions of *n*-octane produce the initial H atom and methyl radicals, but their impact on the product distribution is minor due to the high energy barriers and long characteristic reaction times (>1 sec, see, Fig. S2 of the SPM). The analysis of characteristic

reaction time indicates that with 10 ppm H atom, chosen as a representative radical concentration under the vitiated environment in the flow reactor, the H-abstraction reaction is rate limiting (Fig. 3). Under this condition, the thermal decomposition of *n*-C_8H_{18} produces predominately ethene, followed by propene and 1-butene. The methyl radical and H atom undergo H-abstraction reactions with the fuel to form methane and hydrogen respectively. The secondary reactions yield other species. For example, the recombination of methyl radicals produces ethane, and the decomposition of propene produces propyne and allene. It may be assumed that olefins larger than C_4, e.g., 1-pentene (1-C_5H_{10}), are rapidly converted to C_2H_4 and C_3H_6 under the H-atom assisted, chemically activated reactions: 1-C_5H_{10} + H → C_2H_4 + CCC• → 2C_2H_4 + CH_3, or 1-C_5H_{10} + H → C_3H_6 + CC• → C_3H_6 + C_2H_4 + H. The above discussion qualitatively explains the experimental observations shown in Fig. 2, in that the thermal decomposition of *n*-octane produces a small number of stable species with ethene being the dominant one.

The product distribution can be estimated quantitatively, without the need to write down every elementary reaction. Since the secondary radicals have roughly the same thermochemical properties, they have approximately the same yield upon equilibrium. Following the approach proposed in [1], we let the equilibrated yield be x for each secondary octyl radical. In a generalized form and for C_nH_{2n+1} radicals derived from a corresponding normal alkane, the yield of the primary radical is then $1–(n/2–1)x$ if n is even, and $1–[(n+1)/2–1]x$ if n is odd). The equilibrium of the octyl radicals is independent of pressure; and x is not a function of pressure. It can be a function of temperature, but the actual temperature dependence is weak [1]. The average values of x in the temperature range of 700-1400K are calculated by equilibrium to be 0.31, 0.36, 0.45 for the secondary octyl, heptyl, and hexyl radicals, respectively. Constrained also by the elemental balance, the formation of stable species through the β-scission reactions of each equilibrated radical can thus be determined. The overall rate coefficient used is the sum of those of each radical isomer. An example is provided in Table S1 in SPM to illustrate how some of the rate constants are estimated. Combining all of the factors, the thermal decomposition of *n*-C_8H_{18} can be described simply by two lumped reaction steps as shown in Table 2, in which R• is

mainly H and CH_3 for under the current experimental condition. Under combustion conditions, R• may also include O_2, O, OH, and HO_2. As will be discussed later, by combining the lumped reaction steps with a detailed foundational fuel chemistry model, we are able to reproduce the product distribution shown in Fig. 2 and predict global combustion properties such as ignition delay and flame speed.

Table 2. Lumped reactions of the four octane isomers studied.

		Products							
Reactant(s)		RH	H	CH_3	C_2H_4	C_3H_6	1-C_4H_8	2-C_4H_8	*i*-C_4H_8
n-C_8H_{18}	→		1.2092	0.7908	2.6051	0.5470	0.0895	-	-
n-C_8H_{18} + R•	→	1	0.4199	0.5801	2.0061	0.9081	0.1709	-	-
t-C_8H_{18}	→		1.8040	0.1960	-	-	-	0.0245	1.9265
t-C_8H_{18} + R•	→	1	1	-	-	-	-	-	2
d-C_8H_{18}	→		0.9478	1.0522	0.4688	1.9898	-	-	0.0102
d-C_8H_{18} + R•	→	1	0.5202	0.4798	0.5202	1.5202	-	-	0.4798
i-C_8H_{18}	→		0.8318	1.1682	0.0842	1.0002	-	-	0.9157
i-C_8H_{18} + R•	→	1	0.0011	0.9989	0.1077	0.6279	0.0180	0.0120	1.1956

2,2,3,3-Tetramethylbutane (t-C_8H_{18})

To contrast the reaction pathways of *n*-C_8H_{18}, we next discuss the most branched isomer *t*-C_8H_{18}. Due to its symmetry, all of the H-atoms in *t*-C_8H_{18} are equivalent. After H-abstraction, the resulting alkyl radical undergoes β-scission directly, which preferentially yields isobutene and its precursor, the tertiary butyl radical, as shown in Fig. 4. The initiation reactions of *t*-C_8H_{18} preferentially break a C-C bond that produces two tertiary butyl radicals leading to isobutene formation. Hence, dominant isobutene formation in the thermal decomposition of *t*-C_8H_{18} is an expected outcome, as discussed also in several early studies [19, 20]. The secondary reactions of isobutene can produce propene through the chemically activated reaction *i*-C_4H_8 + H → C_3H_6 + CH_3. Similarly, propene produces ethene through C_3H_6 + H → C_2H_4 + CH_3. The methyl radical generated forms methane by the H-abstraction of *t*-C_8H_{18}. Similar to *n*-C_8H_{18}, a two-step reaction model may be formulated with the product distributions as listed in Table 2.

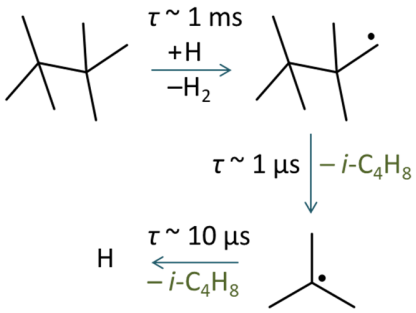

Fig. 4. Reaction paths of *t*-C_8H_{18} thermal decomposition following H-abstraction and C-C β-scission. The characteristic times are calculated for 1000 K temperature, 1 atm pressure with 10 ppm initial H mole fraction. The H atom concentration used in the calculation of the characteristic time is typical for the experiment.

2,5-Dimethylhexane (d-C_8H_{18})

d-C_8H_{18} is the least branched among the three branched isomers studied. The equilibrated radicals dissociate to produce ethene, propene, and isobutene. The initial C-C fission reactions result in a similar group of stable alkene species. The reaction paths shown in Fig. 5 suggest that if the β-scission rate coefficients are equal among the alkyl radicals, the production of propene is dominant, followed by ethene and then isobutene. It may be assumed that the branched C_5 alkene (see, the bottom of Fig. 5) undergo H-assisted decomposition to form ethene and *iso*-propyl, and that the branched C_6 alkene undergoes H-assisted decomposition to form propene and *iso*-butyl radical. Hence, a two-step reaction model may be constructed, as shown in Table 2.

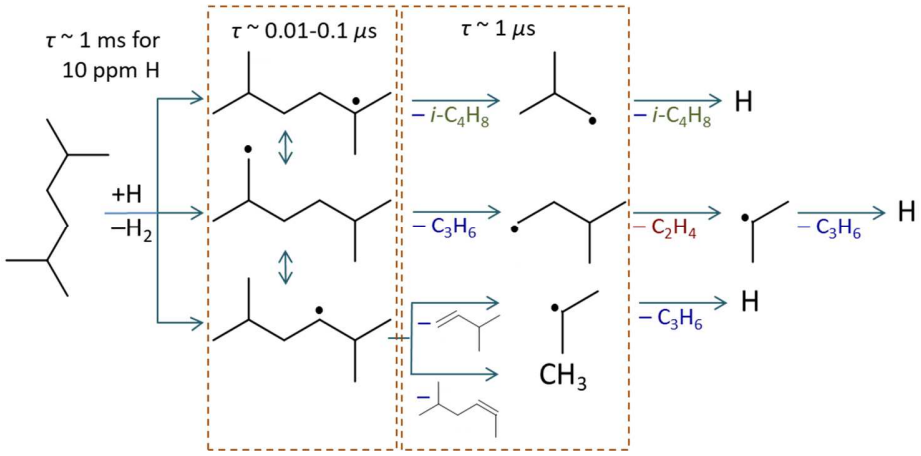

Fig. 5. Reaction paths of *d*-C_8H_{18} thermal decomposition following H-abstraction and C-C β-scission. The characteristic times are calculated for 1000 K, 1 atm with 10 ppm initial H mole fraction. The H atom concentration used in the calculation of the characteristic time (10 ppm) is typical for the experiment.

2,2,4-Trimethylpentane (i-C_8H_{18})

Among the four isomers, *i*-C_8H_{18} has received the most attention. However, very few studies have directly focused on the characterization of intermediate product distribution of fuel pyrolysis. It is seen that for *i*-C_8H_{18}, the formation of propene and isobutene dominate over ethene and methane, though not as significantly as the other three octane isomers (cf. Fig. 2).

As shown in Fig. 6, the H-abstraction reactions can produce four radical isomers, followed by their equilibration and β-scission, basically producing isobutene and propene. The reaction path analysis indicates that *i*-C_8H_{18} produces mostly isobutene and propene. Treating the decomposition of the three branched alkenes by the H-assisted decomposition reactions similar to the C_5 and C_6 alkenes in the *d*-C_8H_{18} analysis, we obtain again a two-step reaction model for *i*-C_8H_{18}, as shown in Table 2.

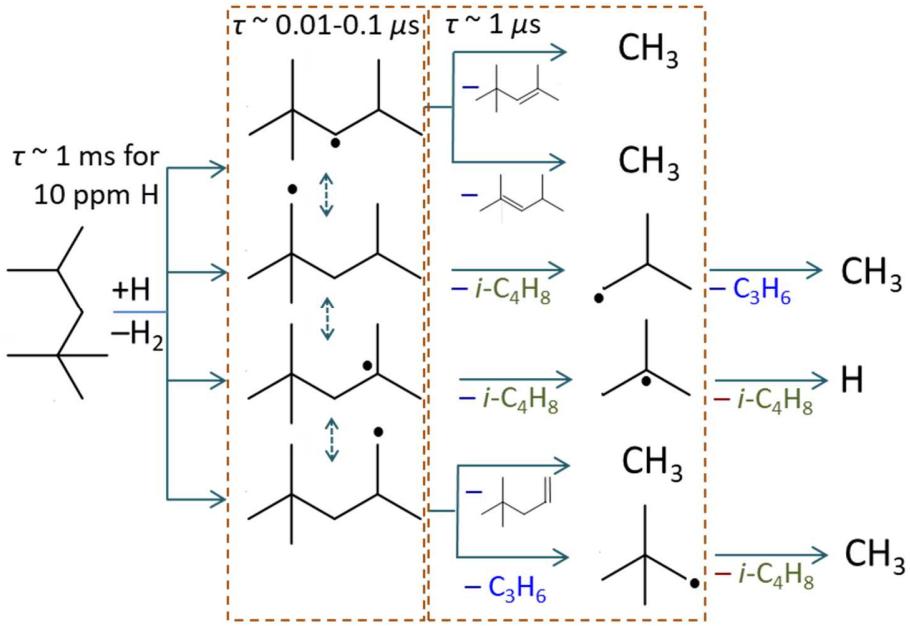

Fig. 6. Reaction paths of *i*-C_8H_{18} thermal decomposition following H-abstraction and C-C β-scission. The characteristic times are calculated for 1000 K, 1 atm with 10 ppm initial H mole fraction. The H atom concentration used in the calculation of the characteristic time (10 ppm) is typical for the experiment.

Discussion

The impact of fuel molecular structure on the pyrolysis product distribution becomes evident from the above analyses. The straight-chain *n*-octane produces predominantly ethene, but no isobutene, while the heavily branched *t*-C_8H_{18} produces predominantly isobutene. For the branched isomer without tertiary carbons (e.g., *d*-C_8H_{18}), the primary product is propene. For the branched isomer with both tertiary and non-tertiary carbons, e.g., *i*-C_8H_{18}, both propene and isobutene are produced in significant amounts. This study did not include a study of lightly-branched isomers, e.g., monomethyl heptane, for which the product distribution may be easily postulated. Comparing *n*-C_8H_{18} and *d*-C_8H_{18}, single methyl substitution should produce predominantly ethene; propene may also be produced in notable amounts.

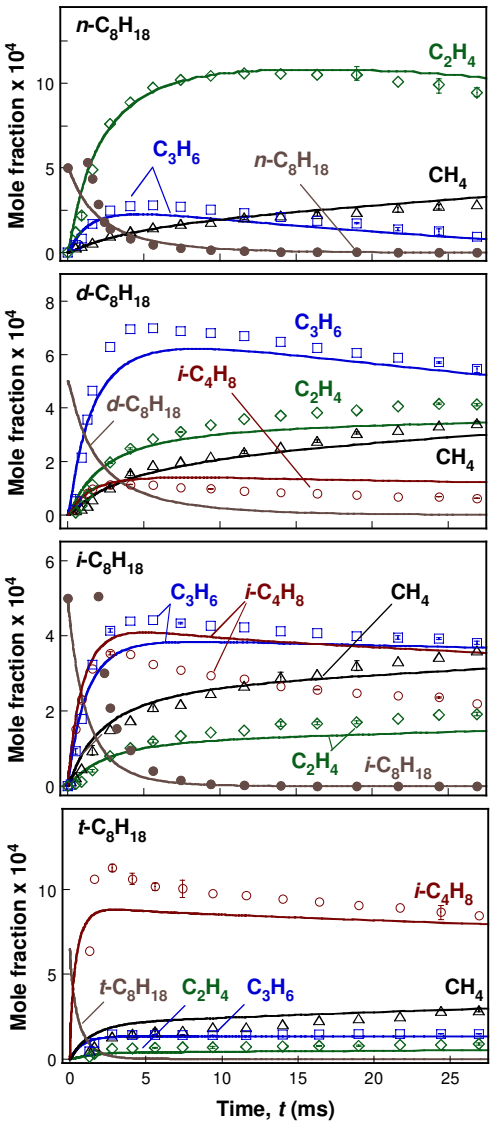

Fig. 7. Experimental (symbols) and computed (lines) species concentrations for the oxidative pyrolysis of the four octane isomers. The vertical bars through the data indicate scatter in multiple experiments.

Characteristic reaction time analyses illustrate that the product distribution is largely thermodynamically controlled. Alkyl radicals of 5 or more carbon atoms, generated by the H-abstraction or initiation C-C fission reactions, tend to reach equilibrium among themselves through the fast H-shift isomerization reactions. The equilibrated radicals then undergo β-scission. Again, controlled by thermodynamics, the same group of stable species are produced in the thermal decomposition of all octane isomers, although some produce more ethene, and others yield more isobutene. In fact, the petroleum-derived jet fuels also produce intermediates similar

to those observed here with benzene and toluene being the additional species [1, 2]. The oxidation of these intermediates then determines the rates of radical chain branching and heat release.

As discussed earlier, two-step reaction models can be derived and are listed in Table 2 for each octane isomer to describe the thermal decomposition. Combined with USC Mech II to account for the secondary reactions, numerical simulations were carried out for all of the experiments conducted. Figure 7 shows the comparison of experimental and simulated species concentration profiles for the four key products. As seen, the agreement is very good considering that only two reaction steps are used to describe the entire process of fuel break down to $C_{1\text{-}4}$ species. The initial shapes of *n*-C_8H_{18} and *i*-C_8H_{18} are influenced by mixing at the reactor inlet; and again, the profiles of *d*-C_8H_{18} and *t*-C_8H_{18} are not measured because they disappear in the first few microseconds. A control simulation was also conducted for *n*-octane decomposition by starting the simulation at a reaction time of 3 ms using measured species concentration as the input of the initial condition. The simulation tests the mixing effects that may impact the initial reaction process. As seen in Fig. S3 of the Supplementary Materials, no appreciable difference is seen when compared to results shown in Fig. 7. To illustrate the relationship between the intermediate species and combustion behaviors, the two-step reaction models are used to predict the ignition delay and flame speed of *n*-C_8H_{18}, *d*-C_8H_{18}, and *i*-C_8H_{18} (no data available for *t*-C_8H_{18}). As shown in Figs. S4-S5, these global combustion properties are accurately captured by the reaction models, which can also be found in the SPM.

Lastly, it is important to note that in our treatment of the reaction models, no data fitting is necessary. The rate parameters of the reactions used are obtained from the fundamental reaction rate coefficients of the corresponding C–C fission of the parent fuel molecules and the β-scission of the respective alkyl radicals.

Conclusions

This study illustrates that the product distributions in the thermal decomposition of four octane isomers are closely related to their molecular structure. The *n*-octane produces mostly ethene, while the most branched isomer, 2,2,3,3-tetramethylbutane, produces predominantly isobutene. Without a tertiary carbon, 2,5-dimethylhexane produces mostly propene; with one tertiary carbon in the molecular structure, *iso*-octane produces both propene and isobutene. The characteristic reaction time and pathway analyses show that under the conditions studied, the H-abstraction reactions are the rate-limiting steps during the oxidative pyrolysis of the octane isomers. The initially generated alkyl radicals reach thermodynamic equilibrium before they undergo β-scission reactions, which are fast compared to the overall reaction time of the experiments. The fact that a two-step reaction scheme, along with a detailed foundational fuel chemistry model, can adequately predict the fuel decay and product distribution for the four octane isomers suggests that, once the reaction paths are understood, the product distribution can be predicted quantitatively without needing to write down every elementary reaction. Furthermore, the modeling results provided a direct and quantitative explanation for the relationship among fuel molecular structure, intermediate products distribution, and global combustion behaviors.

Acknowledgment

K.W. wishes to thank Mr. Yue Zhang and Mr. Rui Xu for their help in setting up the flame speed calculations. This work was supported by the U.S. Air Force Office of Scientific Research under grant numbers FA9550-14-1-0235 and FA9550-16-1-0195, the U.S. Federal Aviation Administration (FAA) Office of Environment and Energy as a part of ASCENT Project 26 under FAA Award Number: 13-C-AJFE-SU-006, and by the National Aeronautics and Space Administration under agreement number 13-C-AJFE-SU-006.

References

[1] H. Wang, R. Xu, K. Wang, C.T. Bowman, D.F. Davidson, R.K. Hanson, K. Brezinsky, F.N. Egolfopoulos, Combust. Flame, 2018, doi.org/10.1016/j.combustflame.2018.03.019.

[2] R. Xu, K. Wang, S. Banerjee, J. Shao, T. Parise, Y. Zhu, S. Wang, A. Movaghar, D.J. Lee, R. Zhao, X. Han, Y. Gao, T. Lu, K. Brezinsky, F.N. Egolfopoulos, D.F. Davidson, R.K. Hanson, C.T. Bowman, H. Wang, Combust. Flame, 2018, doi.org/10.1016/j.combustflame.2018.03.021.

[3] K. Wang, R. Xu, T. Parise, J. K. Shao, D. J. Lee, A. Movaghar, D.F. Davidson, R.K. Hanson, H. Wang, C.T. Bowman, F.N. Egolfopoulos, in: *10th US National Meeting on Combustion*, College Park, MD, 2017.

[4] C.K. Westbrook, W.J. Pitz, J.E. Boercker, H.J. Curran, J.F. Griffiths, C. Mohamed, M. Ribaucour, Proc. Combust. Inst. 29 (2002) 1311-1318.

[5] C.K. Westbrook, W.J. Pitz, H.C. Curran, J. Boercker, E. Kunrath, Int. J. Chem. Kinet. 33 (2001) 868-877.

[6] J.M. Smith, J.M. Simmie, H.J. Curran, Int. J. Chem. Kinet. 37 (2005) 728-736.

[7] E.J. Silke, H.J. Curran, J.M. Simmie, Proc. Combust. Inst. 30 (2005) 2639-2647.

[8] C.S. Ji, S.M. Sarathy, P.S. Veloo, C.K. Westbrook, F.N. Egolfopoulos, Combust. Flame 159 (2012) 1426-1436.

[9] S.M. Sarathy, C. Yeung, R. Gehmlich, C.K. Westbrook, M. Plomer, Z.Y. Luo, M. Mehl, W.J. Pitz, K. Seshadri, M.J. Thomson, T.F. Lu, Proc. Combust. Inst. 34 (2013) 1015-1023.

[10] S. Banerjee, R. Tangko, D.A. Sheen, H. Wang, C.T. Bowman, Combust. Flame 163 (2016) 12-30.

[11] X. You, F.N. Egolfopoulos, H. Wang, Proc. Combust. Inst. 32 (2009) 403-410.

[12] S.J. Klippenstein, Y. Georgievskii, L.B. Harding, Phys. Chem. Chem. Phys. 8 (2006) 1133-1147.

[13] B. Sirjean, E. Dames, H. Wang, W. Tsang, J. Phys. Chem. 116 (2011) 319-332.

[14] K. Wang, S.M. Villano, A.M. Dean, J. Phys. Chem. 119 (2015) 7205-7221.

[15] E. R. Ritter, J.W. Bozzelli, Int. J. Chem. Kinet. 23 (1991) 767-778.

[16] H. Wang, X. You, A.V. Joshi, S.G. Davis, A. Laskin, F.N. Egolfopoulos, C.K. Law, USC Mech Version II: High-temperature combustion reaction model of H_2/CO/C_1-C_4 compounds. http://ignis.usc.edu/Mechanisms/USC-Mech II/USC_Mech II.htm.

[17] R.J. Kee, F.M. Rupley, J.A. Miller, CHEMKIN: A general-purpose, problem-independent, transportable, FORTRAN chemical kinetics code package, Sandia Report SAND-89-8009, Sandia National Laboratories, Albuquerque, N.M., 1989.

[18] A. Ratkiewicz, T.N. Truong, J. Phys. Chem. 116 (2012) 6643-6654.

[19] J.E. Taylor, T.S. Milazzo, Int. J. Chem. Kinet. 10 (1978) 1245-1257.

[20] R.M. Marshall, J.H. Purnell, P.D. Storey, P. Roy. Soc. Lond. A MAT. 363 (1978) 503-523.